



A portable monitoring approach using cameras and computer vision for bridge load rating in smart cities

Chuan-Zhi Dong¹ · Selcuk Bas^{1,2} · F. Necati Catbas¹

Received: 11 February 2020 / Revised: 12 August 2020 / Accepted: 14 August 2020 / Published online: 29 August 2020
© Springer-Verlag GmbH Germany, part of Springer Nature 2020

Abstract

Smart structures require novel, efficient, and effective technologies for their safe operation and serviceability. This paper presents a novel, practical, cost-effective, and field test-based methodology using portable cameras and computer vision technologies to identify the lateral live load distribution factors for the existing highway bridges to perform load rating. By using a computer vision-based measurement method and traffic recognition, the girder deflection under live load can be monitored in a noncontact way and can be utilized to derive the load distribution. To verify the feasibility of the proposed approach, a comparative experimental study is conducted on a real-life pre-stressed concrete bridge with a set of conventional load tests and experiments in normal traffic. The results are compared with the conventional approach, such as simplified formulations recommended by AASHTO specifications, and the experimental method using the data from strain gauges and a calibrated finite element model (FEM). The comparative results show that the proposed approach can obtain very similar load distribution factors and bridge load rating factors both in a conventional load test and normal traffic. In comparison to the simplified formulation recommended by AASHTO specifications, the proposed approach can reflect the real-life structural properties and improve the load rating factor of AASHTO specifications by around 12%. In addition, as compared to the load-test-based approaches, such as using strain data and calibrated FEM, the proposed approach does not require traffic closure and a large amount of effort to deal with the load test and model updating. The bridge studied in this paper represents a very typical one from a large population of bridges that are part of the smart infrastructure. Such a practical approach will be practical and cost-effective for bridge load rating in smart cities.

Keywords Bridge distribution factor · Load rating · Load test · Computer vision · Displacement measurement · Highway bridges

1 Introduction

1.1 Statement of the problem

Bridges are significant components in the transportation systems and play a critical role in the operation of our infrastructures. Ensuring the normal operation of bridge with healthy condition is one of the tasks in the operation, maintenance and management of the infrastructure systems in the

development of our future's smart cities. As indicated in the 2017 Infrastructure Report Card of America released by the American Society of Civil Engineers (ASCE) [1], 40% of the bridges (245,754 out of 614,387) in the US are 50 years old or older, and 9.1% of them (around 56,007) were rated as “structurally deficient” up to 2016. With the aging of the nation's bridges, most of them are approaching the end of their design life [1]. As indicated in the ASCE 2017 Infrastructure Report Card, “the most recent estimate puts the nation's backlog of bridge rehabilitation needs at \$123 billion” [1]. The lack of funds and financial constraints for immediate rehabilitation and renewal of the bridges rated as “structurally deficient” would postpone the progress of the rehabilitation and replacement of the posted bridges. On a worldwide scale, there is also a similar trend. It is becoming more important to objectively evaluate the structural condition and safe load-carrying capacity of bridge structures and

✉ F. Necati Catbas
catbas@ucf.edu

¹ Department of Civil, Environmental, and Construction Engineering, University of Central Florida, Orlando, FL 32816, USA

² Department of Civil Engineering, Bartın University, Bartın, Turkey

prioritize their replacement in the prevention of fatalities and disasters [2]. Recently bridge collapses, such as those that happened in Italy [3], Mainland China [4], and Taiwan [5], also bring the safety issues of bridges into the public concern. The as-is situation gives rise to a pressing need to evaluate the real status of the performance and condition of bridge structures and take measures for efficient bridge management, maintenance, retrofitting, and rehabilitation to prevent catastrophic incidents.

Generally, a regular bridge inspection every two years is mandated by the state's Departments of Transportation (DOTs) and Federal Highway Administration (FHWA) in the US, and the related agencies in the other countries. The biennial bridge inspection relies on the visual inspection which is well accepted and codified throughout the industry. However, it takes a large amount of time, cost, and labor force to do visual inspection, and the results rely heavily on the subjective justifications and experiences of the inspectors. Load rating is one of the important approaches for condition assessment of bridge structures and it can provide a quantitative indicator—rating factor—to evaluate the load-carrying capacity of bridges. Load rating is a measure of safe live load-carrying capacity of a bridge, which is generally used by the bridge owners to perform decision making, including retrofit, repair, and load posting to limit vehicular loading [6]. The basic idea of load rating factor (RF) can be expressed as “ $RF = (\text{Capacity} - \text{Dead load Demand}) / \text{Live Load Demand}$ ”. The calculations of capacity and dead load demand are static problems and can be easily converted to plane analysis according to the properties of dead loads. However, the major challenge is the distribution of vehicular live load on bridges, which is to answer the question of how the live load transfers from a vehicle to the bridge slab and girder sections. Lateral live load distribution is the key when doing advanced analysis for load rating which represents the structural strength and serviceability of bridge structures [7]. The procedure of calculating lateral live load distribution factor is to convert a three-dimensional (3D) load distribution problem to a two-dimensional (2D) or one-dimensional (1D) problem. The way of estimating the live load lateral distribution problems also leads to different methods of load rating.

In current research studies and practices, there are two major types of methods to perform bridge load rating: simplified methods and detailed analysis using finite element model (FEM) methods. In both types of methods, the calculations of distribution factors directly affect the results of the load rating. The simplified methods generally can be used to conduct beamline analysis with lateral distribution, which considers the geometry information of the bridge, such as girder spacing and span length, and the relative stiffness of the slab–girder system. For example, the specifications published by the American Association of State

Highway and Transportation Officials (AASHTO) [8], such as AASHTO standard specifications for highway bridges [9] and AASHTO Load and Resistance Factor Design (LRFD) bridge design specifications [8] summarize the empirical formulas to calculate the lateral live load distribution to perform beamline analysis. Beamline analysis means to analyze a beam/girder over multiple spans under the vehicle load and multiply the response by the distribution factor (DF). The load distribution and load rating calculation presented in AASHTO standard and LRFD specifications [10] provide simplified ways to estimate the load rating capacity in the design stage. During the bridge operation stage, the load distribution and rating still follow the same procedure as stated in the design stage, but the impact factor for demand (related to dead loads and live loads) and the resistance factors (related to capacity) have to be modified based on the wearing surface condition evaluation, field inspection, or maintenance of the structural component members according to the AASHTO Manual for Bridge Evaluation [11] or National Bridge Inspection Standards Regulations (NBIS) [12]. This type of simplified methods derive the results, which are indicated to be more conservative than the actual bridge status [6] and may not incorporate real-structural properties.

The other type of methods, FEM-based load rating, may reflect more about the actual cases of bridge structures than the simplified methods. The lateral live load distribution can be delicately analyzed with FEM, and the load transfer in the lateral section from the vehicle to the slab and then to the girders is much clearer. As the distribution factor is much closer to the actual loading behavior, which means smaller distribution factors as compared to that from the simplified methods, the load rating factor can be increased and the expenses on primary bridge members can be reduced. It can also prevent the earlier load permit posting during the whole bridge operation stage. However, detailed 2D FEMs are necessary for the load rating purposes. This would take large amounts of time, effort, and expertise [6]. To ensure the reliability and accuracy of the FEM, the FEM has to be calibrated/updated by the information from field tests, e.g., static and dynamic load tests [13]. During the load testing, traffic closure, testing truck arrangement, sensor instrumentation, and cable wiring work are required. Although they are routine activities, it would take large amounts of efforts in engineering practices.

It is clear to see that a more simplified, practical, and reasonable approach for estimating bridge distribution factor for load rating is more beneficial for the engineering practices. The bridge load rating for the purpose of structural condition assessment with cost-effective and convenient solutions can provide an important support for the operation compliance of our infrastructure system in the development of future's smart cities.

1.2 Related work

Several previous research studies and engineering practices investigated the lateral live load distribution with simplified and empirical formulations derived from FEM simulation and load testing analysis for various slab–girder configurations. AASHTO standard specifications for highway bridges [9] suggested the simple ratio (S/D) of girder spacing, S , divided by a constant, D , which is related to the bridge type and number of traffic lanes. Although this simple ratio is very easy for the engineers to use, it results in the conservative load estimation and does not estimate the moment and shear values properly for skewed bridges. Zokaie [14] provided more accurate formulations which consider span length, girder stiffness, girder spacing, slab thickness, skew angle, and differences between moment and shear effects. Zokaie's work is also recommended by the AASHTO LRFD bridge design specifications [8]. Nowak et al. [15] calculated the load distribution factors with the experimental data by using two different methods. In the first method, they only took the ratio of the strain at the girder to the sum of all the bottom-flange strains as distribution factor. In the second method, they first calculated the weighted ratio of each girder's section modulus to the sum of the section modulus of all the girders, and the weighted ratio was used to calculate the weighted strain of each girder. Then they obtained the distribution factor of the girder by using the weighted strain. Nowak et al. [15] indicated that the second method considered the difference of section modulus of each girder and showed more uniform distribution in the tests. Eom and Nowak [16] compared the experimental methods using a ratio of girder strain/weighted strain with the formulations recommend by AASHTO standard specifications for highway bridges and AASHTO LRFD bridge design specifications, and found that distribution factors calculated by the proposed experimental method are smaller than the AASHTO specifications, especially the exterior girders. Bar et al. [17] investigated the effects of lifts, skew angle, continuity, diaphragms, and load type on distribution factors by using FEMs. Huo et al. [10] introduced a simple and practical distribution calculation method (Henry's method) which is developed by a former engineer (Henry Derthick) of the Tennessee Department of Transportation (TDOT) and has been used by TDOT in the last 50 years. Henry's method is much simpler to use as compared to the AASHTO LRFD method, and it only requires such information as bridge width, number of traffic lanes, and the number of girders. Chung et al. [18] investigated the effects of deck cracking and the secondary elements on load distribution of steel I-shape girder bridges. Yousif and Hindi [7] investigated the limitations and applicability of the AASHTO LRFD method of load distribution calculation by using 886 FEMs. Li and Chen [19] developed an FEM for live load

distribution calculation which uses elastic spring elements to simulate the reaction of main girders to the deck system, and they proved that this model can be used to compute lateral load distribution without limits to parameters, such as truck–wheel space, span length, and girder space. Hodson et al. [20] calibrated the FEM of a box–girder bridge using data from load test and calculated the load distribution factor and load rating factor by using this calibrated model. Then they conducted a parametric study of this calibrated model by using various parameters, such as skew, girder spacing, parapets, span length, and slab thickness and summarized a new equation for load distribution which predicts more accurate distribution factors of the exterior girder. Catbas et al. [6] proposed a simplified equation for the estimation of the distribution factor by using the regression analysis of bridge skew angle, modal frequency, and flexibility coefficient. In this study, the modal frequency and flexibility coefficient can be easily obtained by a rapid impact test. Jiao et al. [21] introduced a lateral load distribution estimation approach by using the modal flexibility of bridges. However, the modal flexibility obtained in this study was calculated from an FEM. Eamon et al. [22] investigated the load distribution and moment continuity of two pre-stressed concrete I-shaped girder bridges by using load tests and FEMs. Choi et al. [23] conducted an extensive parametric study to determine the distribution factors of two-span multicell box–girder bridges by using 120 FEMs. They found that the number of boxes, the span length, and the number of lanes significantly affect the distribution factors. Based on the parametric study, they proposed a set of equations under AASHTO LRFD methods for the estimation of distribution factors, and the results agree well with that from FEM analysis.

1.3 Objectives and scope

The authors have been exploring how to measure the structural responses by using practical and cost-effective approaches, such as computer vision-based monitoring [24–28]. Without traffic closure and load testing procedure, portable cameras and computer technology can be easily implemented to monitor the bridge deflections/displacement and also estimate by means of a practical field monitoring data the external loads during normal traffic. In some research examples [21, 29] and bridge load testing practices [30], the proportion of girder deflections in the same cross section under live load is applied to calculate the lateral distribution factor. By combining the computer vision-based displacement monitoring approach and the girder deflection-based distribution factor calculation, the distribution factor can be easily obtained by means of a practical field monitoring data. The main objective of this study is to propose a novel, practical, field test-based, cost-effective approach for estimating the bridge

distribution factor for bridge load rating in smart cities, which leads to more efficient load estimations as compared to AASHTO codes/standards/specifications, and also does not require major effort for the development of FEM, load testing, and model updating as compared to FEM-based approaches. In this context, the scope of the paper is given as follows: (1) discuss the estimation of the lateral distribution factor by using girder deflections; (2) introduce a noncontact displacement monitoring method by using portable cameras and computer vision for the calculation of distribution factor; (3) demonstrate comparisons of estimation of the distribution factor and load rating by using AASHTO specifications, FEM with model updating, and the proposed approach during a load test example; and (4) demonstrate an application of estimation of distribution factor and load rating by using the proposed approach in normal traffic.

2 Methodology

2.1 Estimation of distribution factors using displacement

Figure 1 shows the schematic diagram of the estimation of load distribution factors from deflections. A unit load $p = 1$ is imposed on the slab–girder system at the i th girder’s position. Here i is the order number of the girder where the load is imposed. In Fig. 1a, for the purpose of demonstration, $i = 2$ is taken as an example. For the elastic beam, the reaction force $p_{j,i}$ of the j th girder is proportional to the deflection of this girder [21] and it can be represented by

$$p_{j,i} = \alpha_j u_{j,i} \tag{1}$$

where α_j is a proportionality factor for the j th girder. For the slab–girder system for which all the girders have the same cross section and material properties, the proportionality factor is a constant. Here it is denoted by α and Eq. (1) then becomes

$$p_{j,i} = \alpha u_{j,i} \tag{2}$$

According to the reciprocal theorem of displacement, $u_{j,i} = u_{i,j}$, for the reaction force

$$p_{j,i} = p_{i,j} \tag{3}$$

For the slab–girder system with n girders, under the unit load, the static equilibrium can be represented as:

$$\sum_{j=1}^n p_{j,i} = \sum_{i=1}^n p_{i,j} = 1 \tag{4}$$

The vertical coordinate value of the influence line of the lateral load distribution of the i th girder can be represented as:

$$DF_{j,i} = p_{j,i} = p_{i,j} \tag{5}$$

the diagram of the influence line of the lateral load distribution is shown in Fig. 1c.

Combining Eqs. (2) and (4), the constant proportionality factor can be obtained as

$$\alpha = \frac{1}{\sum_j^n u_{j,i}} = \frac{1}{\sum_i^n u_{i,j}} \tag{6}$$

Substituting Eqs. (2) and (6) into Eq. (5), the distribution factor can be expressed as

$$DF_{j,i} = \frac{u_{j,i}}{\sum_j^n u_{j,i}} \tag{7}$$

The distribution factor expressed in Eq. (7) is in a fashion of vertical coordinates of the influence line of lateral load distribution, which means when multiple loads are imposed on the same cross section, such as vehicle loads, the distribution factor can be calculated using superposition operation. In practice, the distribution factor can be calculated by using the measurable deflections and the two different loading scenarios are shown in Fig. 2: single lane loaded and multiple lanes loaded.

The distribution factor of the i th girder using measurable girder deflections can be calculated as following:

$$DF_i = \frac{d_i}{\sum_{k=1}^n d_k} \tag{8}$$

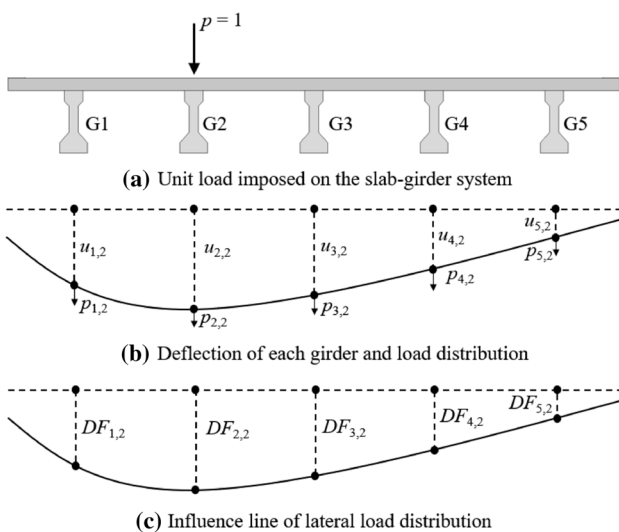


Fig. 1 Schematic diagram of estimation of load distribution factors from deflections

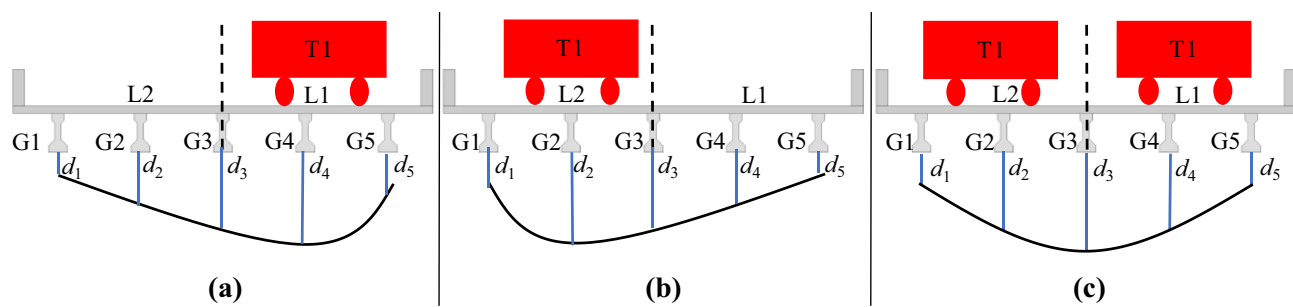


Fig. 2 Distribution factor calculation using measurable girder deflections: **a** truck (T1) on the lane 1 (L1)-single lane loaded; **b** truck (T1) on the lane 2 (L2)-single lane loaded; and **c** two truck-multiple lanes loaded

where k is the girder number, n is the total number of girders, d_i and d_k are the deflections of the i th girder and k th girder, and $k = 1, 2, \dots, i, \dots, n$.

In the next section, the computer vision-based displacement measurement method will be introduced to monitor the girder deflection without major time, cost, labor force, and traffic closure, which makes the estimation of the distribution factor much easier.

2.2 Computer vision-based displacement measurement by using feature matching

The idea of using camera and computer vision technology to measure the displacement is to use the camera to take the video of the measurement region, estimate the motion of the measurement region in the video by using computer vision technologies, such as image registration and visual tracking, and then convert the motion in image to the real-life world [31–37]. Figure 3 shows the flowchart of the computer vision-based displacement measurement method using feature matching.

There are six steps to estimate displacement from the videos or image sequences by using the proposed approach. At first, the camera has to be calibrated in advance and obtain the relationship between the image coordinates and the real world. In other words, it has to find out how many physical units (e.g., millimeter) in the real-world represent a pixel unit in the image dimension. The authors' previous work [24] made a detailed summarization of practical camera calibration approaches. In this study, the scale ratio, SR, is applied as the practical calibration approach and it is formulated as

$$SR = \frac{L}{l} \quad (9)$$

where L is the actual dimension (e.g. height in millimeter, mm) of the object in the real world, and l is the dimension (e.g. height in pixel) of the object in the image. The scale ratio expressed in Eq. (9) is only suitable for the case

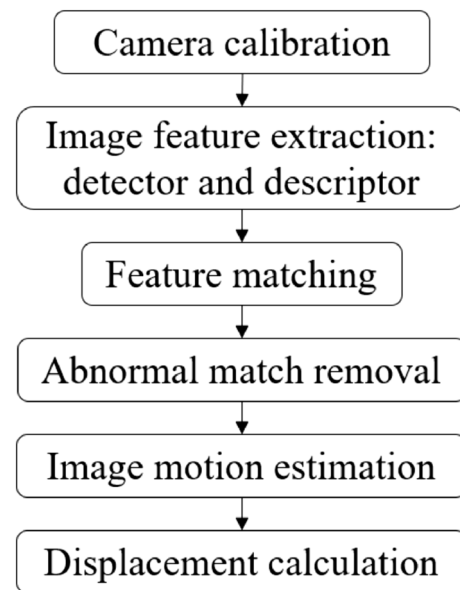


Fig. 3 Flowchart of the computer vision-based displacement measurement method

when the axis of the camera and lens is perpendicular to the motion plane of the measurement target. For the cases that there is an inclination between them, the authors' previous work [28] gives a detailed demonstration that this paper will not repeat.

Secondly, the camera records the video or image sequence of the measurement region. Image features are required to track the motion of the measurement region. An image feature is a specific sub region of the image which in general has some special texture or characteristics. The sub region of the image is also called a feature detector or key point (kp). Also, the feature descriptor is required to represent the feature detector mathematically. The feature descriptor is usually a vector. Dong et al. [28] summarized the pros and cons of different feature detectors and descriptors. Dong and Catbas [27] found that it improved 24% of the measurement accuracy by using SIFT (scale-invariant feature transform)

feature detector and VGG (Visual Geometry Group in University of Oxford) descriptor than by using the original SIFT feature detector and descriptor, which is a very popular feature extraction algorithm in computer vision. In this study, SIFT feature detector and VGG descriptor are implemented.

Thirdly, the feature matching is conducted between the images in the video or image sequence, as shown in Fig. 4. The feature matching is actually to find the two most similar features in two images. To estimate the similarity, the distance of the descriptors of the two features are calculated and the smallest distance indicates the best similarity. After the initial feature matching, there might be some abnormal matches, which are apparently wrong matches, as shown in Fig. 4a. The fourth step is to remove the abnormal matches. In this study, the RANSAC (RANDOM SAMPLE CONSENSUS) method is implemented to remove the abnormal matches. Figure 4b shows the feature matching after abnormal match removal.

In the next step, the image motion, in other words, the location change of the measurement region, can be estimated by calculating the average feature location change in all the matches. In this stage, the location change of the measurement region is in the dimension of the image pixel. At the end, the actual displacement in x and y directions, X and Y in physical units, can be calculated by

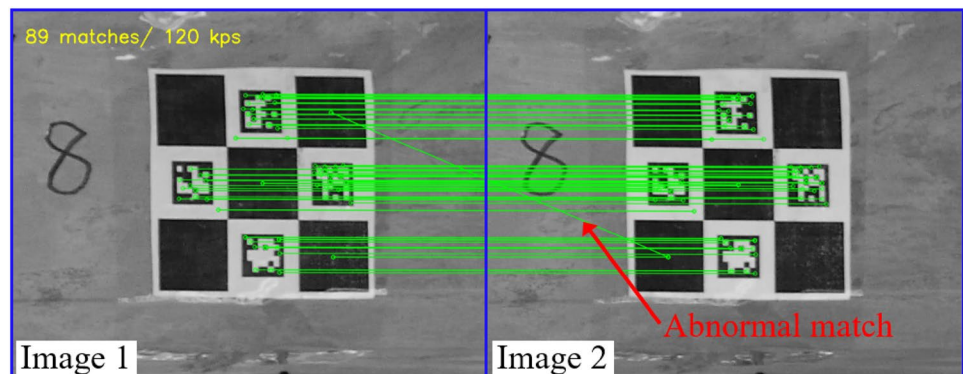
$$\begin{cases} X = SR_x \frac{\sum_{v=1}^m (x_u^v - x_1^v)}{m} \\ Y = SR_y \frac{\sum_{v=1}^m (y_u^v - y_1^v)}{m} \end{cases} \quad (10)$$

where (x_u^v, y_u^v) and (x_1^v, y_1^v) are the image coordinates of the v th matched feature point between the measurement region of the u th image and the first image, m is the total number of the matched feature point between the u th image and the first image, and SR_x and SR_y are the scale ratios in the x and y directions.

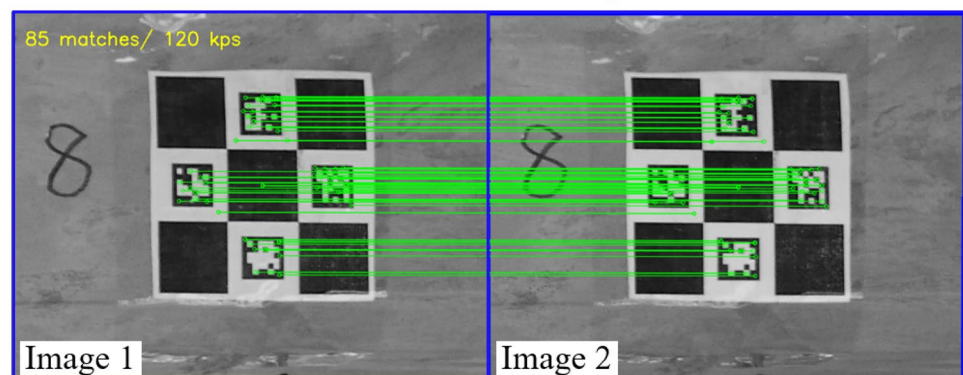
2.3 Calculation of load rating factor

With the displacement measured by using the computer vision-based displacement measurement method as listed in Eq. (10), the lateral girder distribution factors formulated in Eq. (7) by using girder deflections can be calculated. Then the vehicle loads can be allocated to each girder from the slab, and the live load (LL) on each girder for load rating can be determined. The load rating factor is calculated by using the equation below:

Fig. 4 Feature matching and abnormal match removal



(a) Feature matching



(b) After abnormal match removal

$$RF = \frac{\phi_c \phi_s \phi R - \gamma_{DC} DC - \gamma_{DW} DW \mp \gamma_p P}{\gamma_L (LL + IM)} \quad (11)$$

where ϕ is the load and resistance factor design (LRFD) resistant factor, ϕ_s is the system factor for redundancy, ϕ_c is the optional member condition factor which is based on the visual inspections, R is the structure resistance, DC is the dead load, DW is the wearing surface load, P is the pre-stress load, LL is the live load, IM is the impact effect, and γ_{DC} , γ_{DW} , γ_p , and γ_L are the factors for different loads. A detailed explanation can be found in AASHTO LRFD Bridge Design Specifications [8]. In this paper, the load rating factor of moment is selected for the demonstration and R , DC , DW , P , LL , and IM in Eq. (11) refer to moments.

3 System configuration

The proposed approach is implemented as a portable system and the system consists of a set of portable cameras, a set of synchronization modules, a computer, and a suite of software as shown in Fig. 5. In the portable cameras, one camera is applied to record the traffic on the bridge and recognize which lane is loaded and the other cameras are applied to monitor the deflection of the bridge girders in the same cross

section. The synchronization module is used to synchronize all the cameras. All the video footages are transferred to the computer and analyzed to extract the lateral load distribution factor and then load rate the bridge.

4 Experimental verification and field application on a real-life bridge

4.1 General features of the bridge

As shown in Fig. 6, the bridge in the study is a multi-span pre-stressed concrete bridge. The bridge was constructed in 1964 and has a total length of 2993 ft (912 m). Each span consists of five pre-stressed I-beams (AASHTO Type II girders). The total length of each span is 52 ft (15.85 m) and the width is 33.08 ft (10.08 m). The girders are spaced at 6.5 ft (1.98 m). The thickness of the slab is 7 in. (17.8 cm). In this experiment, only the first span is considered, and all the experiments were conducted for the first span.

4.2 Experimental setup

To verify the proposed approach, two sets of experiments are conducted: (1) conduct the general load test (static loading)

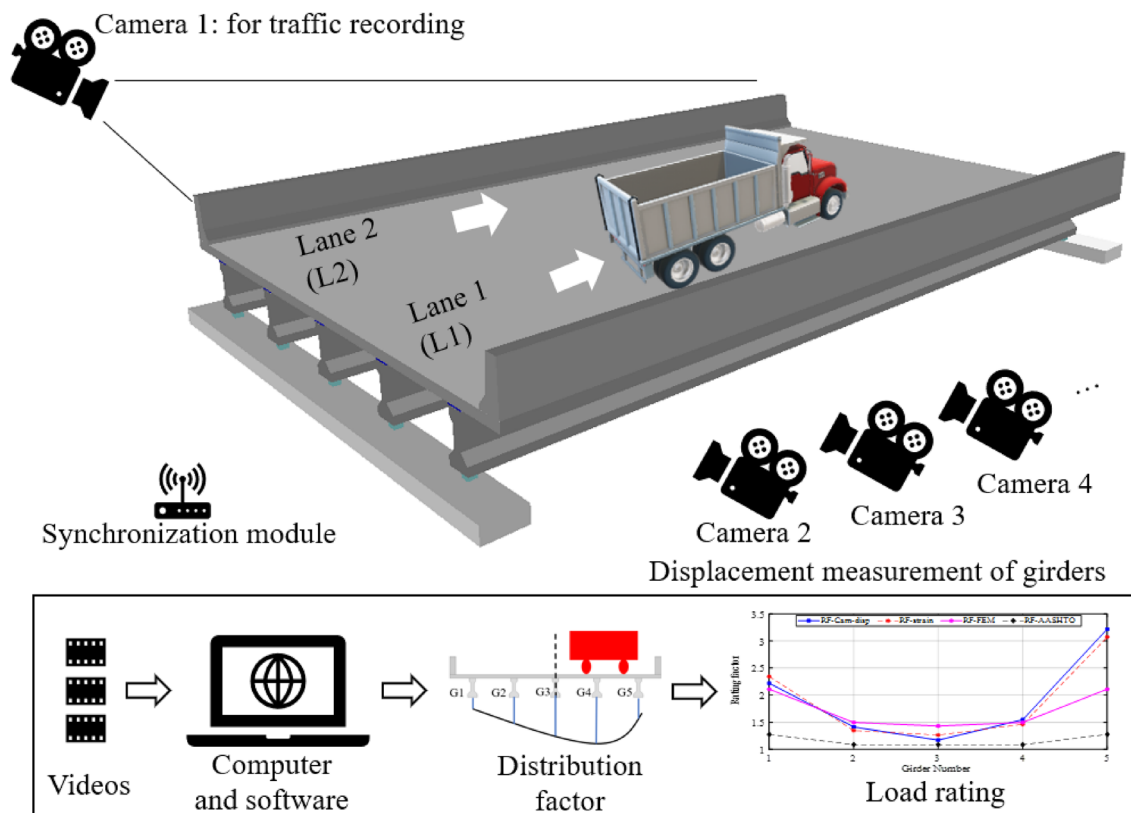


Fig. 5 System configuration

Fig. 6 The pre-stressed concrete highway bridge in this study



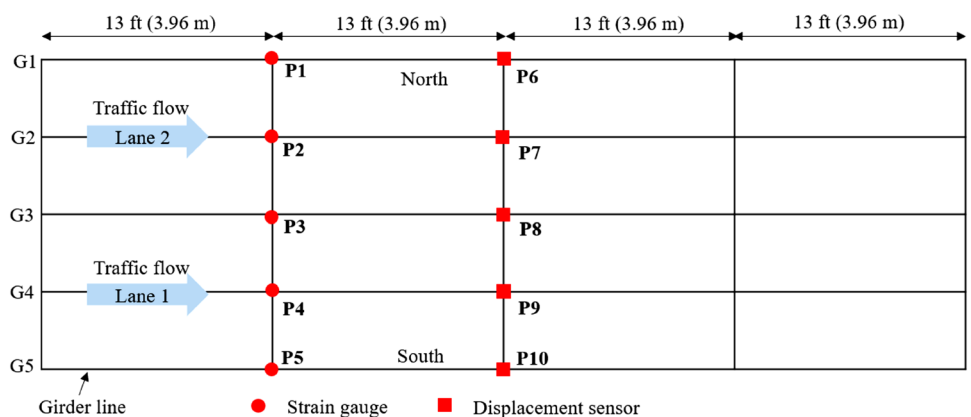
in the conventional way and compare the results of the proposed approach with AASHTO methods, strain method, and FEM method; (2) conduct the experiment in normal traffic and verify the proposed approach. The main setup of the two sets of experiments are similar. As shown in Fig. 7, two types of sensors were installed on the bridge. Five displacement sensors (i.e., potentiometers) were installed at the mid span of each girder to measure the displacement. Three cameras (Z CAM E1, 4K, 30 FPS, 75–300 mm zoom lens) were employed to measure the displacements at the same location. The first camera recorded the motion of Girder 1 (G1) and Girder 2 (G2), the second camera recorded the motion of Girder 3 (G3) and Girder 4 (G4), and the third camera recorded the motion of Girder 5 (G5). Five strain gauges were installed at the 1/4 span of each girder. One camera (Canon VIXIA HF R42) was employed to record the traffic footage. Figure 8 shows the sensors, including displacement sensor and strain gauge, and cameras used in this study. Figure 9 gives more details about the instrumentation of different sensors and cameras. In Fig. 9a, the manual markers were attached on the side surface of the girders, and they were regarded as targets for visual tracking when

using vision-based displacement measurement methods. The manual marker installed here is ChArUco Diamond, which is a chessboard composed of 3×3 squares and 4 ArUco markers and very commonly used in computer vision [38].

The two sets of experiments were conducted as four cases and are listed in Table 1. The first two cases are the load test cases, as stated before, and they are static tests. The last two cases are to use the normal traffic, and they are dynamic tests.

Figure 10 shows the truck employed in this study. As shown in Fig. 10a, the truck was manually instructed to be arranged on the specific positions during the load tests of Case 1 and Case 2. Figure 10b gives an example of the static truck loading status on the bridge. Figure 11 illustrates the truck loading configuration. Figure 12 shows the loading plan of the static tests. In the static loading cases, the truck (T1) was loaded at four different locations on the first span of the bridge with four steps. In each step, the truck stopped for a certain amount of time and then slowly moved to the next location. In Case 1 (T1L1), the truck was loaded on Lane 1 (L1), and in Case 2 (T1L2), the truck was loaded on Lane 2. In Case 3 and Case 4, during the dynamic test and

Fig. 7 Sensor instrumentation plan



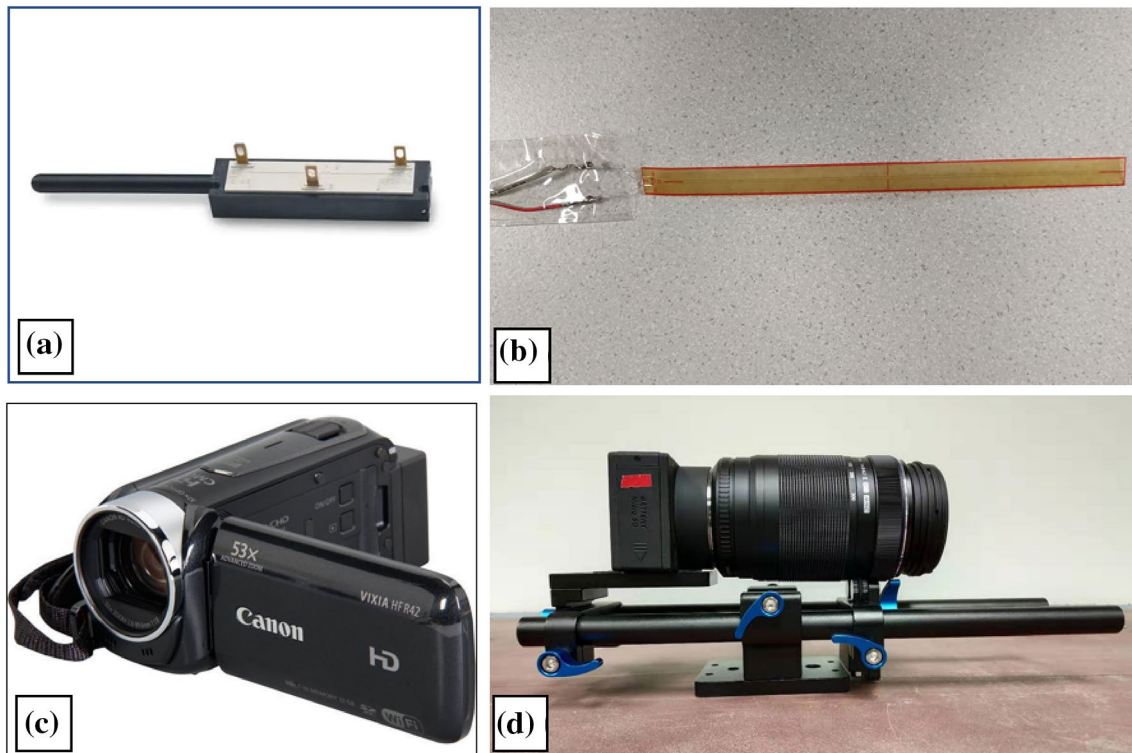


Fig. 8 Sensors and cameras used in the test: **a** displacement sensor (potentiometer), **b** strain gauge, **c** camera for traffic monitoring, and **d** camera for displacement measurement

normal traffic, the truck crossed the first span of the bridge with a speed of 35 miles per hour (mph) on Lane 1 and Lane 2, respectively. In the dynamic test, the truck moving load is regarded as the normal traffic load. During the experiment, the sensors and cameras recorded the responses of the first span of the bridge, and the videos from the Canon camera were regarded as a reference to check the truck loading.

4.3 Result analysis

4.3.1 Result of the conventional load test (static tests): Case 1 and Case 2

Figure 13 shows the displacement result of each girder of the mid-span of Case 1 (TIL1, static). The displacement data is obtained from the camera and displacement sensor (potentiometer). During the experiment, the displacement sensors (potentiometers) installed at Girder 1 and Girder 5 went through some problems. This might be because the base of the potentiometers had some small motions. Since the deflections of the exterior girders are quite small, the small motions impacted the measurement results of the potentiometers at Girder 1 and Girder 5. This is also one of the issues of contact type measurement of the conventional displacement sensors. The comparison between the displacement data from cameras and potentiometer is only within Girder 2, Girder 3, and Girder

4. From the displacement time histories, it can be seen that the displacement of each girder under this truck load is quite small and all of them are within 1 mm. The results from the camera using a computer vision-based method are raw data, and no filtering is applied. From Fig. 13, it can be seen that the displacement results from the proposed approach are very consistent with that from the conventional displacement sensors. This proves that the proposed noncontact type displacement measurement method by using a camera and computer vision can give reliable results and also does not experience the problems that occurred with the potentiometers at Girder 1 and Girder 5. In this study, the distribution factor calculation by the displacement method is conducted by using the displacement data from cameras. Since this is a four-step static loading test, the deflections at each step can be extracted to calculate the distribution factor. In this study, the deflections at the second step (marked as a green bounding box in Fig. 13) are selected to calculate the distribution factor. The distribution factor using displacement data is calculated by Eq. (8).

The distribution factor using strain data is followed by the equation proposed by Nowak et al. [15] and it is expressed as

$$DF_i = \frac{\varepsilon_i}{\sum_{j=1}^n \varepsilon_j} \quad (12)$$



Fig. 9 Sensors and camera instrumentation details for the experiment

where ϵ_i is the strain of the i th girder. The distribution factor calculated by using strain data here refers to the moment distribution factor. Due to the limit of the paper length, the strain time history of each girder is not listed here and the calculated distribution factors by strain data are shown directly. It should be noted that although the strain data is collected at the 1/4 span of the bridge, it still can reflect the lateral load distribution effects of the bridge. To compare with the distribution factor recommended by AASHTO specifications, the equations from AASHTO LRFD Bridge Design Specifications are also used, as listed in Table 2. In this study, an FEM, as shown in Fig. 14, is also used for the estimation of load distribution and load rating. The

distribution factor is calculated by taking the ratio of each girder's moment at midspan to the sum of the moments of all girders at midspan from the FEM. The FEM is calibrated with static and dynamic test data. Details can be found in the authors' previous work [39].

Figure 15 shows the distribution factors calculated from the static load cases. Figure 15a, b are calculated from the cases when only one lane is loaded by a truck. By using the superposition method, the distribution factors when two trucks are loaded on two lanes in the same cross section at the same time are obtained, as shown in Fig. 15c. Figure 15c also refers to the case in AASHTO specifications "Two or more (multiple) design lanes," which is mentioned in Table 2.

Table 3 lists the distribution factors of the static cases. Here the "m" in the item "DF-Cam-m" means "Two or more (multiple) design lanes," and "Cam" means camera. From Fig. 15 and Table 3, it can be seen that when using the AASHTO specifications to calculate the distribution factor, it gives more conservative results and distributes more live load on each girder, especially the girders away from the girder in the centerline (Girder 3). The distribution factors

Table 1 Experimental cases

| Case | Case name | Lane | Loading type |
|------|-----------|-------------|-------------------|
| 1 | TIL1 | Lane 1 (L1) | Static, four-step |
| 2 | TIL2 | Lane 2 (L2) | Static, four-step |
| 3 | TIL1-35 | Lane 1 (L1) | Dynamic, 35 mph |
| 4 | TIL2-35 | Lane 2 (L2) | Dynamic, 35 mph |



Fig. 10 Truck loading on the bridge

calculated from the displacement data (camera), strain data, and calibrated FEM show a very consistent trend and give close results, and all of them are smaller than the results calculated from the AASHTO specifications. In particular, the method from AASHTO specifications allocates too much load to the exterior girders, while the proposed approach and the experimental approach by using strain data and FEM give a more reasonable load allocation.

Also, the proposed approach can reflect the load distribution effects of single lane load and multiple lane load, which is more reasonable for real application and is verified by the other experimental approach by using strain data and FEM. From the comparison results of the static load test, it is feasible to apply the proposed approach for the estimation of the live load lateral distribution factor.

With the extracted distribution factor in Fig. 15 and Table 3, the bridge load rating factors can be calculated by following the AASHTO specifications, as stated in Eq. (11). In general, there are two kinds of load rating: inventory rating and operating rating. The inventory rating corresponds to the design levels of safety recommended by AASHTO specifications and the operating rating corresponds to the upper bound of allowable safety level [40]. The difference is related to the factors of Eq. (11). Both can reflect the load-carrying capacity.

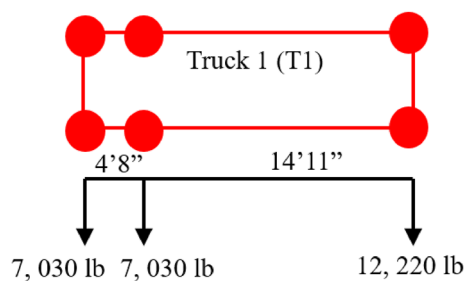


Fig. 11 Truck loading configuration

In this study, the load rating refers to the inventory rating. In the calculation of the rating factor, the truck used here is HL93 and the impact factor is 33%. Figure 16 and Table 4 show the load rating factors extracted from the static load cases. In the single lane load cases, the rating factors of the interior girders and the exterior girder close to the loading lane are comparable when using different methods. The rating factors of the exterior girders which are away from the loading lane are larger when using the proposed approach (13.16 and 38.58) and strain data (48.74 and 42.26) as compared to AASHTO specifications (1.27). One of the possible reasons is that when using the proposed approach and the strain data to obtain the rating factors, only single lane load is considered. However, when using AASHTO specifications, two lane loads are considered. When using measurement-based methods (the proposed approach and the strain data) in single lane load cases, the load distribution effects on the exterior girders which are away from the loading lane are smaller than that calculated by AASHTO specifications. The smaller load distribution effects lead to smaller load distribution factors, which result in higher load rating factors as compared to AASHTO specifications and FEM. The differences are smaller when two/multiple lane loads are considered. As shown in Table 4, when two lane loads are considered by using the proposed approach and the strain data, the rating factors are 3.22 and 3.07, respectively, which are comparable to that calculated by AASHTO specifications (1.27) and FEM (2.11). When compared with the rating factor results obtained from the proposed approach by using cameras and computer vision, the experimental approach by using strain data and the calibrated FEM, it can be seen that the rating factors using the distribution factors calculated from AASHTO specifications underestimate the structural load-carrying capacity. The comparison results also prove that it is feasible to use cameras and the vision-based displacement measurement methods to estimate the

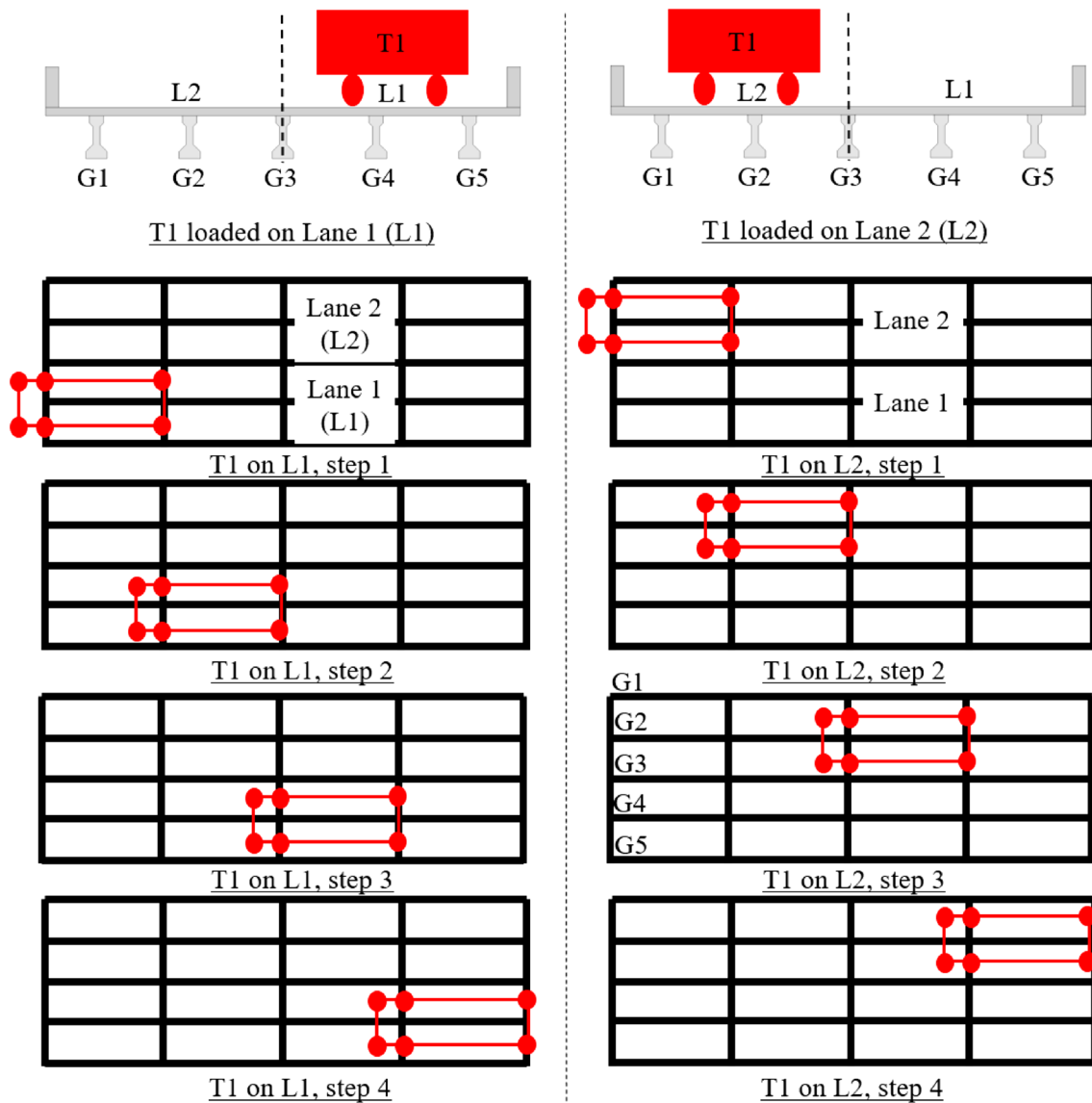


Fig. 12 Loading plan of the conventional load test (static tests)

distribution factors for load rating purposes in the conventional load test (static test).

4.3.2 Result of the experiments during normal traffic (dynamic tests): Case 3 and Case 4

Although the results of the conventional load test prove that it is feasible to use the proposed approach to estimate the lateral live load distribution factors for load rating, it is still not enough to showcase the core competence and major advantages of the proposed approach. The major contribution of

this study is to estimate the lateral live load distribution factors for load rating without load test and traffic closure. It will save time, cost, and labor if the distribution factors can be estimated by using normal traffic and a field test-based approach. This section will prove this concept.

Figure 17 shows the synchronized deflection of the mid-span of each girder. From the camera for traffic recording, it can be seen that a truck crossed the bridge on Lane 1 with a speed of 35 miles per hour (mph). By taking the maximum value of the deflection of each girder (in the blue circle of Fig. 17), the distribution factors can be calculated, which is shown in Fig. 18a. Figure 18b shows

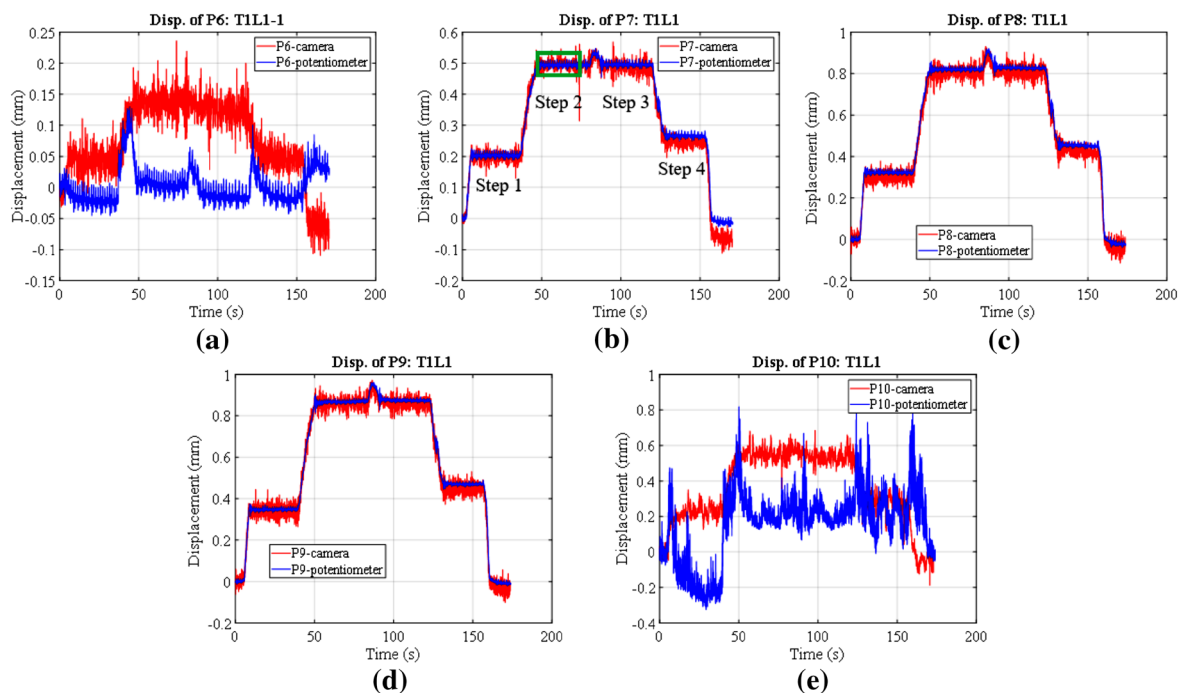


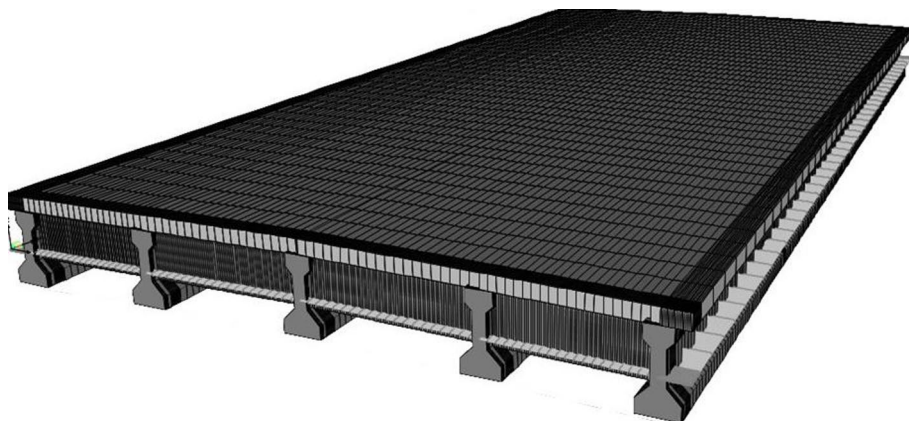
Fig. 13 Displacement results of the midspan of Case 1 (TIL1, static): a Girder 1, b Girder 2, c Girder 3, d Girder 4 and e Girder 5

Table 2 Distribution factor calculation in AASHTO

| DF for moment, interior girder | DF for moment, exterior girder |
|---|---|
| One design lane loaded: $m_{\text{moment}}^{\text{SI}} = 0.06 + \left(\frac{S}{14}\right)^{0.4} \left(\frac{S}{L}\right)^{0.3} \left(\frac{K_g}{12L_s^3}\right)^{0.1}$ | One design lane loaded: $m_{\text{moment}}^{\text{SE}} = \frac{5.5}{S}$ |
| Two or more (multiple) design lanes loaded: $m_{\text{moment}}^{\text{MI}} = 0.075 + \left(\frac{S}{9.5}\right)^{0.6} \left(\frac{S}{L}\right)^{0.2} \left(\frac{K_g}{12L_s^3}\right)^{0.1}$ AASHTO 4.6.2.2.2b-1 | Two or more (multiple) design lanes loaded: $m_{\text{moment}}^{\text{ME}} = e(m_{\text{moment}}^{\text{MI}})$ $e = 0.77 + \frac{d_e}{9.1} \geq 1.0$ d_e is positive if girder is inside of barrier, otherwise negative AASHTO 4.6.2.2.2.1d-1 |

S =girder spacing (ft); L =span length (ft); t_s =slab thickness (in.); $K_g = n(I_g + e_g^2 A)$; n =modular ratio of girder and deck; I_g =moment of inertia of girder (in.⁴), e_g =girder eccentricity which is the distance from girder centroid to middle centroid of slab, (in.); A =girder area (in.²)

Fig. 14 The calibrated finite element model (FEM)



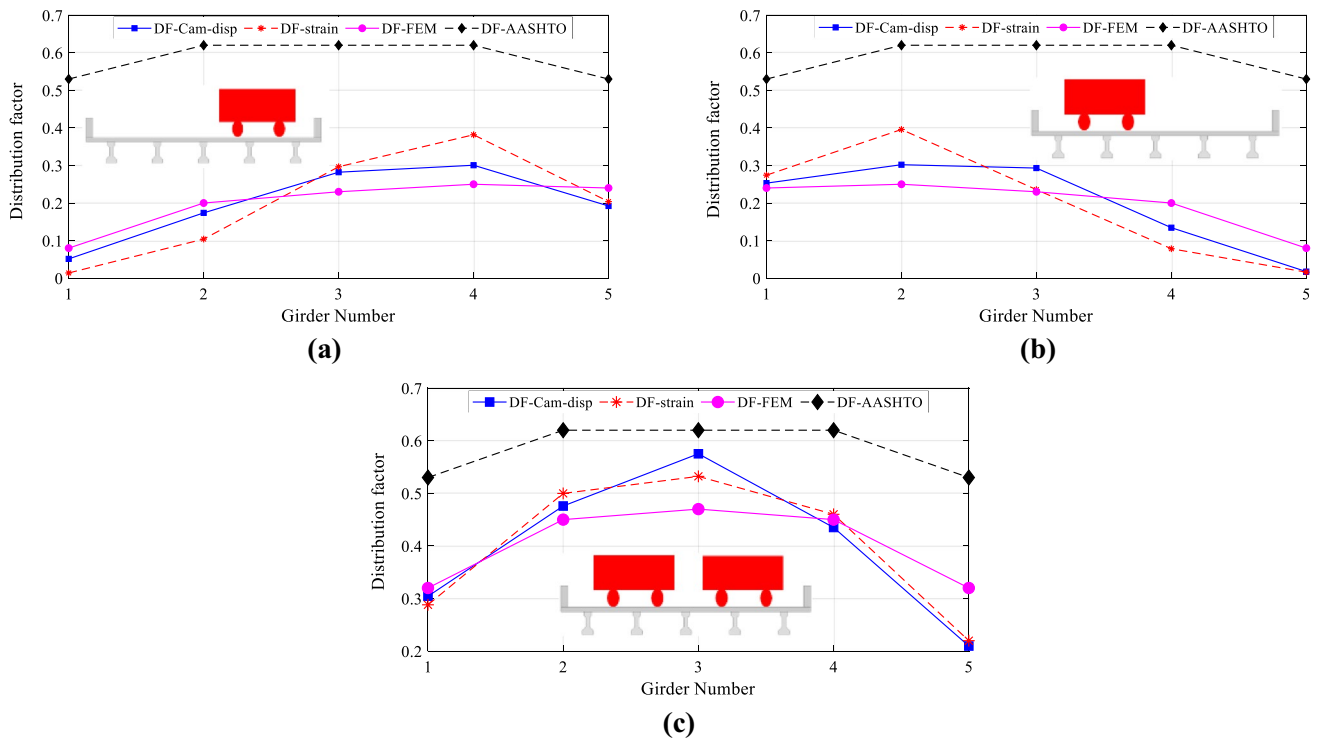


Fig. 15 Distribution factor calculated from the static test cases: **a** Case 1: truck in lane 1, **b** Case 2: truck in lane 2, and **c** two same trucks in both lanes

the distribution factors of the case when a truck crossed the bridge on Lane 2, and Fig. 18c shows the distribution factors when two trucks crossed the bridge on two lanes; they are calculated by the superposition of Fig. 18a, b. In Fig. 18 and Table 5, the distribution factors obtained from the proposed approach (camera and computer vision) are very close to that obtained from FEM. In addition, the distribution factor results obtained in normal traffic are very similar to the conventional load test. The proposed approach gives more reasonable results as compared to the AASHTO specifications, which give much more conservative results.

Figure 19 and Table 6 show the load rating factors calculated with the extracted distribution factors. The load rating factors obtained from the proposed approach in the normal traffic are very close to the results from FEM and very similar to the results from conventional load tests. When compared with the observation that the load rating factor calculated by using the distribution factors from AASHTO specifications underestimates the bridge carrying capacity, the proposed approach gives more reasonable and acceptable estimation. Figure 19c also shows that when considering

multiple lane loads and using three different approaches including camera, FEM and AASHTO, the midspan of G3 always has the smallest load rating factors. Here the midspan of G3 can be regarded as the critical location for the load rating and it can be regarded as example to demonstrate the comparison of three different methods. By calculating the difference from Table 6, it shows that the proposed approach improved the load rating factor by 12% as compared to AASHTO specifications. Although, the load rating factor obtained by the proposed approach is 15% smaller than FEM, it is acceptable to apply the proposed approach in real-life bridge load rating.

4.4 Considerations for engineering practice

Based on the result analysis above, the proposed approach by using cameras and computer vision can provide more reasonable estimation results of load distribution and bridge load rating as compared to AASTHO specifications. It should be noted that the proposed approach is a field-based method and the estimation is based on the data measured from real bridge during normal traffic. When compared

Table 3 Distribution factor calculated from the static test cases

| Girder | DF-Cam-TIL1 | DF-Cam-TIL2 | DF-strain-TIL1 | DF-strain-TIL2 | DF-FEM-TIL1 | DF-FEM-TIL2 | DF-Cam-m | DF-Strain-m | DF-FEM-m | DF-AASHTO |
|--------|-------------|-------------|----------------|----------------|-------------|-------------|----------|-------------|----------|-----------|
| 1 | 0.051 | 0.253 | 0.014 | 0.274 | 0.080 | 0.240 | 0.304 | 0.288 | 0.320 | 0.530 |
| 2 | 0.174 | 0.302 | 0.104 | 0.396 | 0.200 | 0.250 | 0.476 | 0.500 | 0.450 | 0.620 |
| 3 | 0.282 | 0.293 | 0.297 | 0.236 | 0.230 | 0.230 | 0.575 | 0.532 | 0.470 | 0.620 |
| 4 | 0.301 | 0.134 | 0.382 | 0.078 | 0.250 | 0.200 | 0.435 | 0.460 | 0.450 | 0.620 |
| 5 | 0.192 | 0.018 | 0.204 | 0.016 | 0.240 | 0.080 | 0.210 | 0.220 | 0.320 | 0.530 |

with the conventional load rating approach which needs a detailed FEM and a series of elaborate load test, the proposed approach can provide a cost-effective alternative solution for engineering practice. A rough estimate of the field test in this study in terms of cost, time, and labor forces could give a view of the comparison for reference:

(1) Conventional load test. The cost of the sensors including accelerometers, strain gauges, displacement sensors, cables and data acquisition systems is over twenty thousand of US dollars. The load test needs a group of dump trucks and it is necessary to pay for the arrangement of dump trucks. Before the load test, it took at least one day to complete work of the sensor instrumentation and cable wiring. It also took one day to conduct the load test. In the load test, a team of engineers is also necessary to coordinate the whole load test. In addition, it also takes days to develop and update the FEM then perform the load rating analysis based on the updated FEM. In the procedure of FEM analysis, not only the time and labor forces, but also the use of a suite of commercial software for FEM will also increase the total cost.

(2) The proposed approach. The cameras used in this study are consumer-grade cameras and the total cost of the three cameras are about 2000 US dollars. During the experiment, the sensors, cables and data acquisition systems are not necessary. The experiment is conducted in normal traffic and the cost of dump truck arrangement in conventional load test is not necessary. And there is no need to close the traffic which also reduces the cost. The preparation of the camera set-up can be completed within an hour. The test for image data acquisition can also be completed within an hour. Two engineers can conduct the test. The software for the image data analysis in this study is developed by the authors' group and it only took hours to analyze the image data, estimate the distribution factors and calculate the load rating factors.

From the comparison of the rough cost estimates of the conventional load test and the proposed approach, it can be seen that the proposed approach requires less cost, time, and labor forces to complete the load rating task. The proposed approach by using consumer-grade cameras and computer vision techniques could provide a cost-effective alternative solution to support engineering practices in the development of smart infrastructures. On the other side, the proposed approach improves the load rating of the simplified method recommended by AASHTO specifications, but it could not match performance of the detailed load rating by using conventional load test and FEM. The proposed approach could provide an alternative solution for practical load rating with which the performance is between the simplified method recommended by AASHTO specifications and the detailed FEM with conventional load test. The bridge owners, management departments and other agencies can get benefit from the proposed approach by using portable cameras and computer vision to conduct a rapid bridge load rating

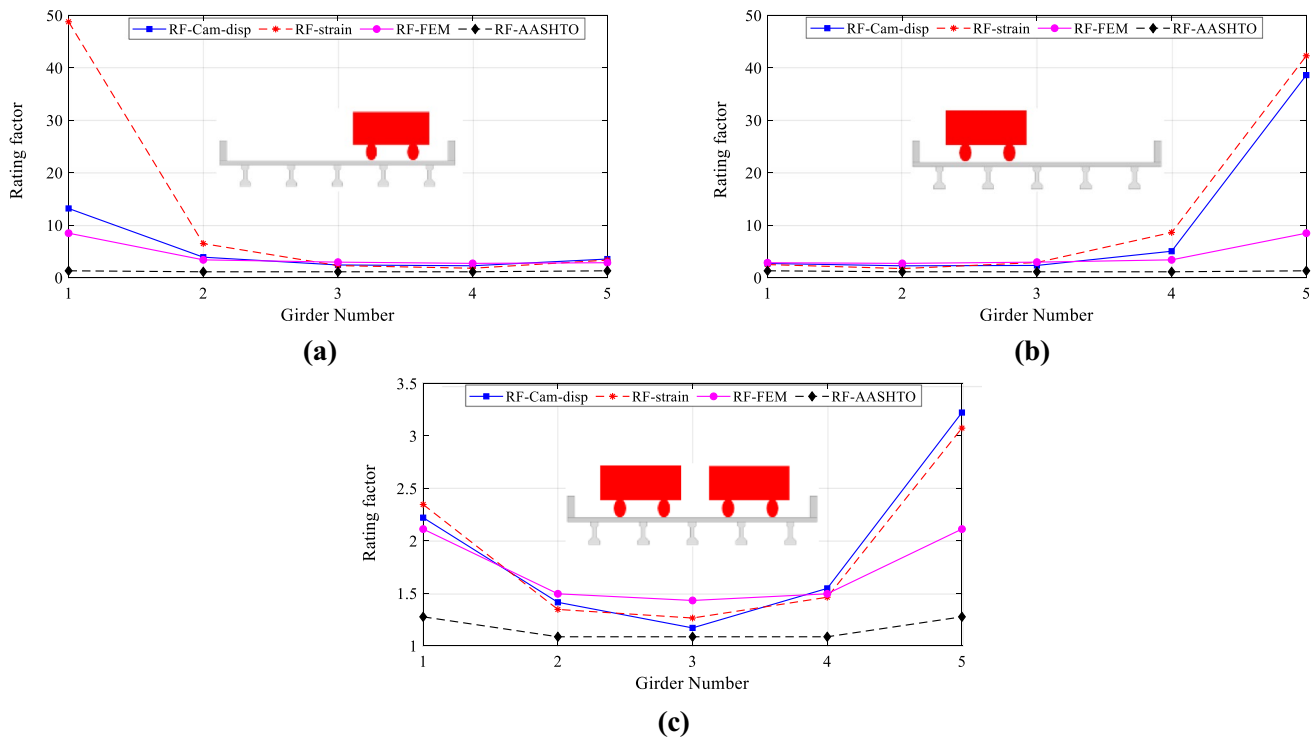


Fig. 16 Load rating factor calculated from the static test cases: **a** Case 1: truck in lane 1, **b** Case 2: truck in lane 2, and **c** two same trucks in both lanes

analysis with field-based measurement data before investing a large amount of efforts including cost, time, and labor force to carry out an elaborate and detailed load test for the bridge load rating purposes.

As a noncontact and optical method, the proposed approach highly relies on the quality of the collected images. The environmental factors, such as light change, partial occlusion, ground motion, wind, etc. might affect the performance of the proposed approach [41]. The adverse environmental factors can reduce the image quality and have influence on the measurement accuracy. In field application, the proposed approach also requires that there are enough visual features or textures on the surface of the structure to track the structural motion for displacement measurement. For the cases without enough visual features, manual markers are necessary. In addition, the camera shaking induced by ground vibration or wind could also result in measurement errors. This problem can be eliminated by subtracting the motion of the static reference on the background in the camera field of view. To obtain more accurate and reliable

bridge rating results and better serve the engineering practices, these considerations should be taken into account and compiled as the instructions for portable implementations of user-friendly software applications.

5 Conclusions

To overcome the inconveniences and disadvantages of the conventional approaches of estimation for the lateral live load distribution factors for bridge load rating in the development of smart cities, in this study a field test-based, practical, noncontact, and cost-effective approach for the estimation of load distribution using portable cameras and computer vision is proposed. The feasibility of the proposed approach is verified through the comparative experimental study on a real life pre-stressed concrete bridge with a set of conventional load tests and experiments in normal traffic. The results are compared with the conventional approach, such as simplified formulations recommended

Table 4 Load rating factor calculated from the static test cases

| Girder | RF-Cam-TIL1 | RF-Cam-TIL2 | RF-strain-TIL1 | RF-strain-TIL2 | RF-FEM-TIL1 | RF-FEM-TIL2 | RF-Cam-m | RF-strain-m | RF-FEM-m | RF-AASHTO |
|--------|-------------|-------------|----------------|----------------|-------------|-------------|----------|-------------|----------|-----------|
| 1 | 13.16 | 2.67 | 48.74 | 2.46 | 8.44 | 2.81 | 2.22 | 2.35 | 2.11 | 1.27 |
| 2 | 3.87 | 2.23 | 6.46 | 1.70 | 3.36 | 2.70 | 1.41 | 1.35 | 1.49 | 1.08 |
| 3 | 2.38 | 2.29 | 2.27 | 2.85 | 2.92 | 2.92 | 1.17 | 1.26 | 1.43 | 1.08 |
| 4 | 2.24 | 5.00 | 1.76 | 8.58 | 2.70 | 3.36 | 1.55 | 1.46 | 1.49 | 1.08 |
| 5 | 3.52 | 38.58 | 3.31 | 42.26 | 2.81 | 8.44 | 3.22 | 3.07 | 2.11 | 1.27 |

by AASHTO specifications and an experimental method by using data from strain gauges and a calibrated FEM. The main approaches, findings, and conclusions are as follows:

(1) This study introduces a practical approach to estimate the load distribution by using measurable girder deflection and influence line of lateral load distribution by means of computer vision.

(2) This study proposes a computer vision-based displacement measurement method using image feature matching, which can conduct noncontact measurement of girder deflection over a long distance. The proposed noncontact displacement measurement method can be implemented for the estimation of the lateral live load distribution and bridge load rating.

(3) The proposed approach can give a more reasonable lateral live load distribution estimation as compared to the conservative load distribution obtained by the formulations provided by the AASHTO LRFD Bridge Design Specifications. The formulations provided by AASHTO are simplified but may not incorporate real-structural properties. The proposed approach is field test-based and can reflect the real-structural properties.

(4) When compared with the approach which requires load test and a large amount of effort to calibrate a detailed FEM, the proposed approach needs less time, cost, and labor force, and does not need to close traffic to complete the test. It avoids many of the challenges present in a conventional load test.

(5) When compared with the approach of using strain data to calculate the load distribution, the proposed approach is a noncontact type method and it does not require sensor instrumentation and cable wiring work, which is much more convenient in practice.

(6) The proposed approach can give reasonable load distribution results and can give higher load rating factors by 12% as compared to AASHTO specifications. Although the load rating factor from the proposed approach is lower than the result from FEM by 15%, considering comparison of the time, cost and labor force, it is viable to apply the proposed approach in real-life bridge load rating.

The proposed approach for the estimation of the lateral live load distribution and bridge load rating provides a very practical, cost-effective and field test-based way to estimate the load distribution effects and load-carrying capacity. The proposed approach also demonstrates a convenient sensing and monitoring solution for the development of sustainable infrastructures in smart cities. The tested bridge in this study represents a very typical population of bridges in our infrastructure systems and it is very promising to promote the proposed approach for further engineering practices of bridge load rating in the future.

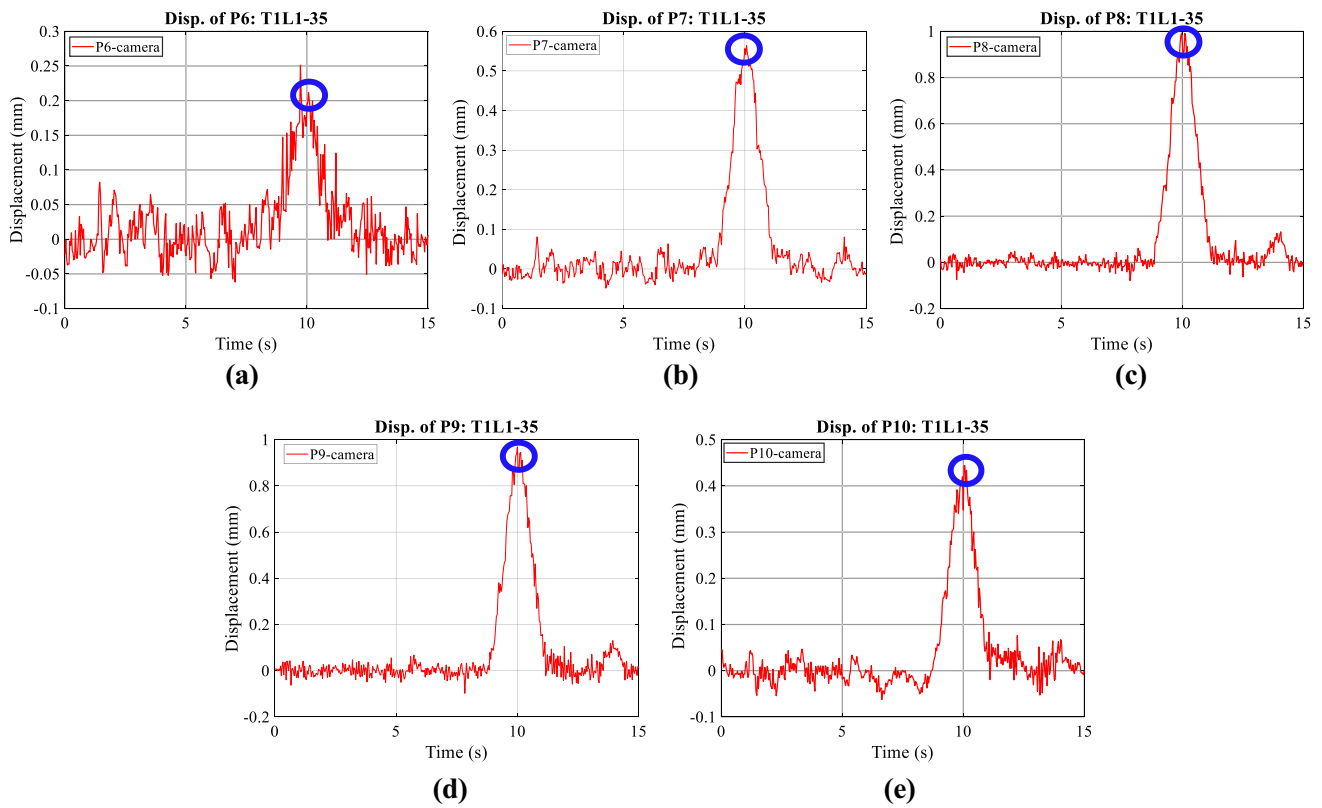


Fig. 17 Displacement results of the midspan of Case 3 (T1L1-35, dynamic): a Girder 1, b Girder 2, c Girder 3, d Girder 4 and e Girder 5

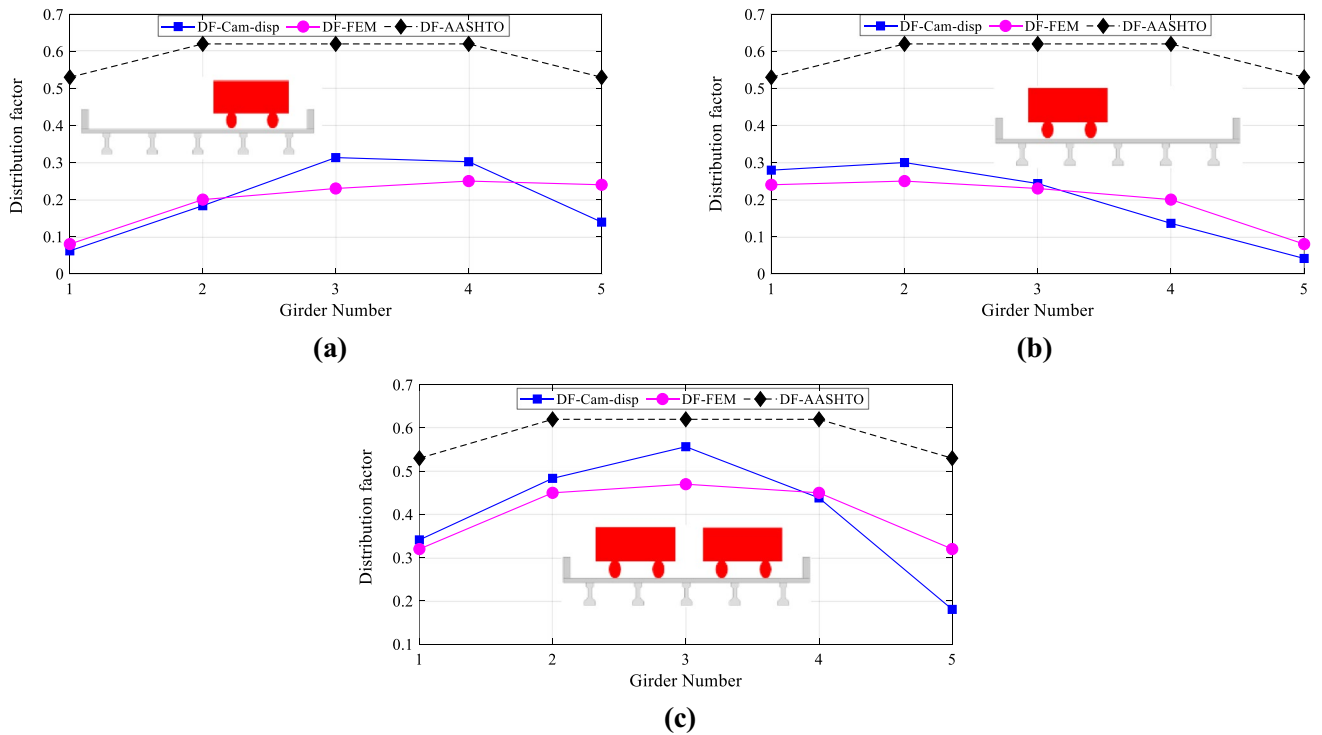


Fig. 18 Distribution factor obtained from normal traffic (dynamic cases): a Case 3: truck in lane 1, b Case 4: truck in lane 2, and c two same trucks in both lanes

Table 5 Distribution factor obtained from normal traffic (dynamic cases)

| Girder | DF-Cam-T1L1 | DF-Cam-T1L2 | DF-FEM-T1L1 | DF-FEM-T1L2 | DF-Cam-m | DF-FEM-m | DF-AASHTO |
|--------|-------------|-------------|-------------|-------------|----------|----------|-----------|
| 1 | 0.062 | 0.279 | 0.080 | 0.240 | 0.341 | 0.320 | 0.530 |
| 2 | 0.183 | 0.300 | 0.200 | 0.250 | 0.483 | 0.450 | 0.620 |
| 3 | 0.313 | 0.243 | 0.230 | 0.230 | 0.557 | 0.470 | 0.620 |
| 4 | 0.302 | 0.136 | 0.250 | 0.200 | 0.438 | 0.450 | 0.620 |
| 5 | 0.139 | 0.041 | 0.240 | 0.080 | 0.180 | 0.320 | 0.530 |

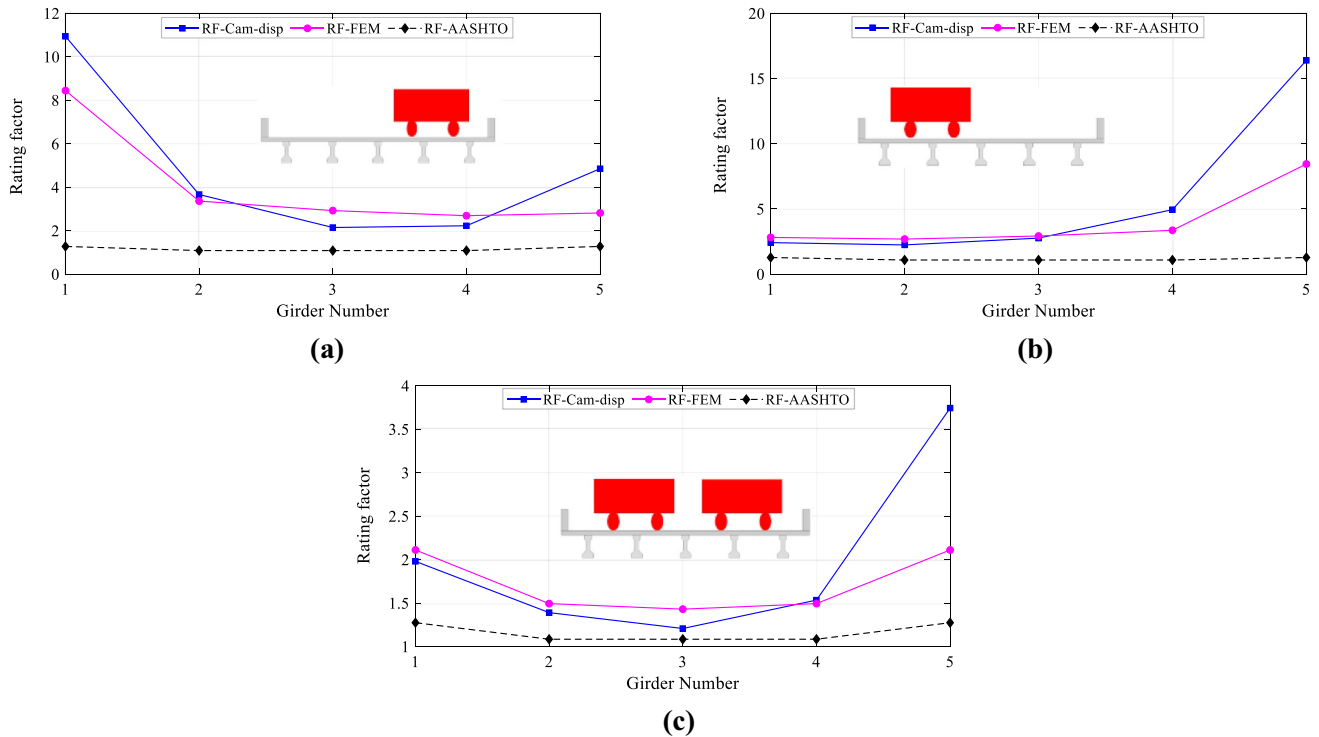


Fig. 19 Load rating factor obtained from normal traffic (dynamic cases): **a** Case 3: truck in lane 1, **b** Case 4: truck in lane 2, and **c** two same trucks in both lanes

Table 6 Load rating factor obtained from normal traffic (dynamic cases)

| Girder | RF-Cam-T1L1 | RF-Cam-T1L2 | RF-FEM-T1L1 | RF-FEM-T1L2 | RF-Cam-m | RF-FEM-m | RF-AASHTO |
|--------|-------------|-------------|-------------|-------------|----------|----------|-----------|
| 1 | 10.94 | 2.42 | 8.44 | 2.81 | 1.98 | 2.11 | 1.27 |
| 2 | 3.66 | 2.24 | 3.36 | 2.69 | 1.39 | 1.49 | 1.08 |
| 3 | 2.15 | 2.76 | 2.92 | 2.92 | 1.21 | 1.43 | 1.08 |
| 4 | 2.22 | 4.94 | 2.69 | 3.36 | 1.53 | 1.49 | 1.08 |
| 5 | 4.85 | 16.39 | 2.81 | 8.44 | 3.74 | 2.11 | 1.27 |

Acknowledgements The financial support for this research was provided by U.S. National Science Foundation (NSF) Division of Civil, Mechanical and Manufacturing Innovation (Grant number 1463493). The authors would like to acknowledge members of the Civil Infrastructure Technologies for Resilience and Safety (CITRS-<https://www.cece.ucf.edu/citrs/>) at University of Central Florida for their endless

support in the creation of this work. The second author would like to kindly acknowledge the Scientific and Technological Research Council of Turkey (TUBITAK) through Grant number 2219. The authors would like to acknowledge Ms. Kaile’a Moseley for her support in editing this paper.

References

- ASCE (2017) 2017 ASCE infrastructure report card. <https://www.infrastructurereportcard.org/making-the-grade/report-card-history/>
- Catbas F, Ciloglu SK, Aktan AE (2005) Strategies for load rating of infrastructure populations: a case study on T-beam bridges. *Struct Infrastruct Eng* 1:221–238. <https://doi.org/10.1080/15732470500031008>
- News B (2018) Italy bridge collapse: what we know so far. <https://www.bbc.com/news/world-europe-45193452>
- Reuters (2019) China bridge collapse kills three, injures two. <https://www.reuters.com/article/us-china-bridge-collapse-idUSKBN1WQ021>
- CNN (2019) Taiwan bridge collapses, sending truck plunging onto fishing boats. <https://www.cnn.com/2019/10/01/asia/taiwan-bridge-collapse-intl-hnk-scli/index.html>
- Catbas FN, Gokce HB, Gul M (2012) Practical approach for estimating distribution factor for load rating: demonstration on reinforced concrete T-beam bridges. *J Bridg Eng* 17:652–661. [https://doi.org/10.1061/\(ASCE\)BE.1943-5592.0000284](https://doi.org/10.1061/(ASCE)BE.1943-5592.0000284)
- Yousif Z, Hindi R (2007) AASHTO-LRFD live load distribution for beam-and-slab bridges: limitations and applicability. *J Bridg Eng* 12:765–773. [https://doi.org/10.1061/\(ASCE\)1084-0702\(2007\)12:6\(765\)](https://doi.org/10.1061/(ASCE)1084-0702(2007)12:6(765))
- AASHTO (2014) AASHTO LRFD bridge design specifications. American Association of State Highway and Transportation Officials, Washington, D.C.
- AASHTO (2002) Standard specifications for highway bridges, 17th edn. American Association of State Highway and Transportation Officials, Washington, D.C.
- Huo XS, Wasserman EP, Zhu P (2004) Simplified method of lateral distribution of live load moment. *J Bridg Eng* 9:382–390. [https://doi.org/10.1061/\(ASCE\)1084-0702\(2004\)9:4\(382\)](https://doi.org/10.1061/(ASCE)1084-0702(2004)9:4(382))
- AASHTO (2018) The manual for bridge evaluation, 3rd edn. American Association of State Highway and Transportation Officials, Washington, D.C.
- FHWA (2004) National bridge inspection standards regulations (NBIS). *Fed Regist* 69:15–35
- Sanayei M, Reiff AJ, Brenner BR, Imbaro GR (2016) Load rating of a fully instrumented bridge: comparison of LRFR approaches. *J Perform Constr Facil* 30:1–7. [https://doi.org/10.1061/\(ASCE\)CF.1943-5509.0000752](https://doi.org/10.1061/(ASCE)CF.1943-5509.0000752)
- Zokaie T (2000) AASHTO-LRFD live load distribution specifications. *J Bridg Eng* 5:131–138. [https://doi.org/10.1061/\(ASCE\)1084-0702\(2000\)5:2\(131\)](https://doi.org/10.1061/(ASCE)1084-0702(2000)5:2(131))
- Nowak AS, Kim S, Stankiewicz PR (2000) Analysis and diagnostic testing of a bridge. *Comput Struct* 77:91–100. [https://doi.org/10.1016/S0045-7949\(99\)00188-1](https://doi.org/10.1016/S0045-7949(99)00188-1)
- Eom J, Nowak AS (2001) Live load distribution for steel girder bridges. *J Bridg Eng* 6:489–497. [https://doi.org/10.1061/\(ASCE\)1084-0702\(2001\)6:6\(489\)](https://doi.org/10.1061/(ASCE)1084-0702(2001)6:6(489))
- Barr PJ, Eberhard MO, Stanton JF (2001) Live-load distribution factors in prestressed concrete girder bridges. *J Bridg Eng* 6:298–306. [https://doi.org/10.1061/\(ASCE\)1084-0702\(2001\)6:5\(298\)](https://doi.org/10.1061/(ASCE)1084-0702(2001)6:5(298))
- Chung W, Liu J, Sotelino ED (2006) Influence of secondary elements and deck cracking on the lateral load distribution of steel girder bridges. *J Bridg Eng* 11:178–187. [https://doi.org/10.1061/\(ASCE\)1084-0702\(2006\)11:2\(178\)](https://doi.org/10.1061/(ASCE)1084-0702(2006)11:2(178))
- Li J, Chen G (2011) Method to compute live-load distribution in bridge girders. *Pract Period Struct Des Constr* 16:191–198. [https://doi.org/10.1061/\(ASCE\)SC.1943-5576.0000091](https://doi.org/10.1061/(ASCE)SC.1943-5576.0000091)
- Hodson DJ, Barr PJ, Halling MW (2012) Live-load analysis of posttensioned box-girder bridges. *J Bridg Eng* 17:644–651. [https://doi.org/10.1061/\(ASCE\)BE.1943-5592.0000302](https://doi.org/10.1061/(ASCE)BE.1943-5592.0000302)
- Jiao Y, Liu H, Wang X, Luo G (2015) Modal property-based approach for lateral distribution evaluation of intact and damaged reinforced concrete bridge. In: *Structural health monitoring 2015*. Destech Publications
- Eamon CD, Chehab A, Parra-Montesinos G (2016) Field tests of two prestressed-concrete girder bridges for live-load distribution and moment continuity. *J Bridg Eng* 21:1–12. [https://doi.org/10.1061/\(ASCE\)BE.1943-5592.0000859](https://doi.org/10.1061/(ASCE)BE.1943-5592.0000859)
- Choi W, Mohseni I, Park J, Kang J (2019) Development of live load distribution factor equation for concrete multicell box-girder bridges under vehicle loading. *Int J Concr Struct Mater* 13:1–14. <https://doi.org/10.1186/s40069-019-0336-1>
- Dong CZ, Celik O, Catbas FN et al (2020) Structural displacement monitoring using deep learning-based full field optical flow methods. *Struct Infrastruct Eng* 16:51–71. <https://doi.org/10.1080/15732479.2019.1650078>
- Dong CZ, Celik O, Catbas FN et al (2019) A robust vision-based method for displacement measurement under adverse environmental factors using spatio-temporal context learning and Taylor approximation. *Sensors* 19:3197. <https://doi.org/10.3390/s19143197>
- Dong CZ, Bas S, Catbas FN (2019) A completely non-contact recognition system for bridge unit influence line using portable cameras and computer vision. *Smart Struct Syst* 24:617–630
- Dong CZ, Catbas FN (2019) A non-target structural displacement measurement method using advanced feature matching strategy. *Adv Struct Eng* 22:3461–3472. <https://doi.org/10.1177/1369433219856171>
- Dong CZ, Celik O, Catbas FN (2019) Marker free monitoring of the grandstand structures and modal identification using computer vision methods. *Struct Heal Monit* 18:1491–1509
- Fanouf F, May J, Wipf T (2011) Development of live-load distribution factors for glued-laminated timber girder bridges. *J Bridg Eng* 16:179–187. [https://doi.org/10.1061/\(ASCE\)BE.1943-5592.0000127](https://doi.org/10.1061/(ASCE)BE.1943-5592.0000127)
- Fan L (2012) Bridge engineering, 2nd edn. China Communication Press
- Dong CZ (2019) Investigation of computer vision concepts and methods for structural health monitoring and identification applications. University of Central Florida
- Chen Y, Joffre D, Avitabile P (2018) Underwater dynamic response at limited points expanded to full-field strain response. *J Vib Acoust* 140:051016. <https://doi.org/10.1115/1.4039800>
- Zhong F, Indurkar PP, Quan CG (2018) Three-dimensional digital image correlation with improved efficiency and accuracy. *Meas J Int Meas Confed* 128:23–33. <https://doi.org/10.1016/j.measurement.2018.06.022>
- Zhong F, Kumar R, Quan C (2019) A cost-effective single-shot structured light system for 3D shape measurement. *IEEE Sens J* 19:7335–7346. <https://doi.org/10.1109/jsen.2019.2915986>
- Tian L, Pan B (2016) Remote bridge deflection measurement using an advanced video deflectometer and actively illuminated LED targets. *Sensors (Switzerland)* 16:1–13. <https://doi.org/10.3390/s16091344>
- Brownjohn JMW, Xu Y, Hester D (2017) Vision-based bridge deformation monitoring. *Front Built Environ* 3:1–16. <https://doi.org/10.3389/fbuil.2017.00023>
- Lee JJ, Fukuda Y, Shinozuka M et al (2007) Development and application of a vision-based displacement measurement system

- for structural health monitoring of civil structures. *Smart Struct Syst* 3:373–384. <https://doi.org/10.12989/sss.2007.3.3.373>
38. OpenCV (2020) Detection of diamond markers. In: Open source computer vision. https://docs.opencv.org/master/d5/d07/tutorial_charuco_diamond_detection.html
39. Dong CZ, Bas S, Debees M et al (2020) Bridge load testing for identifying live load distribution, load rating, serviceability and dynamic response. *Front Built Environ* 6:1. <https://doi.org/10.3389/fbuil.2020.00046>
40. TRB (2019) Primer on bridge load testing. Transportation research circular E-C257, Washington, D.C.
41. Dong CZ, Catbas FN (2020) A review of computer vision-based structural health monitoring at local and global levels. *Struct Health Monit*. <https://doi.org/10.1177/1475921720935585>

Publisher's Note Springer Nature remains neutral with regard to jurisdictional claims in published maps and institutional affiliations.